Composites Part A 112 (2018) 186–196

Contents lists available at ScienceDirect

Composites Part A

journal homepage: www.elsevier.com/locate/compositesa

# Facile fabrication and performance of robust polymer/carbon nanotube coated spandex fibers for strain sensing

Qin Chen[a], Dong Xiang[a,*], Lei Wang[a], Yuhao Tang[a], Eileen Harkin-Jones[b], Chunxia Zhao[a], Yuntao Li[a,*]

[a] School of Materials Science and Engineering, Southwest Petroleum University, Chengdu 610500, China
[b] School of Engineering, University of Ulster, Jordanstown BT37 0QB, UK

ARTICLE INFO

*Keywords:*
A:carbon nanotubes
A:fibers
B:Electrical properties
E:human motion monitoring

ABSTRACT

The last decade has witnessed a tremendous growth of research and development in flexible and wearable strain sensors. However, there are still some challenges associated with the fabrication of strain sensors to achieve a high sensitivity and large workable range at low cost. Here, we report on the development of a highly elastic strain sensor based on a commercial spandex fiber coated with a nanocomposite consisting of multi-walled carbon nanotubes (MWCNTs) and thermoplastic polyurethane (TPU) manufactured by a layer-by-layer (LBL) method. The sensor demonstrated outstanding performance with large workable strain, high sensitivity, excellent repeatability and regular signal responses within a wide measuring frequency range of 0.01–1 Hz. Additionally, the effect of ultraviolet irradiation on the sensor performance was also investigated. Application of the sensor in monitoring diverse human motions, such as facial micro expressions and speech recognition, are also demonstrated showing its potential for applications in wearable devices and intelligent robots.

## 1. Introduction

Much work has been focused on the development of skin-mountable and wearable electronic devices due to their potential for real time and remote monitoring for human health and safety applications. Such devices have also promising application potential for wearable equipment, damage detection, flexible consumer electronics, healthcare, smart human-machine interactions, etc. In addition, stretchable strain sensors play an important role in the artificial sensory system for robots in touch sensing, joint movement monitoring and speech recognition. As a key component of such electronic devices, strain sensors should be mechanically flexible to meet the complex application conditions [1]. Although traditional strain sensor based on metals and semiconductors can be cost-effective, the majority of them are not suitable as wearable sensor due to their rigidity, brittleness [2], low sensitivities and narrow workable range below 5% [1].

To overcome these shortcomings, several types of flexible strain sensors have been reported and typically consist of electrically conductive nanomaterials incorporated into elastic and stretchable polymer matrices. Nanofillers used in these applications include carbon black (CB) [3,4], carbon nanotubes (CNTs) [5–8], graphene [9–12], graphene nanoplatelets (GNPs) [13], nanowires (NWs) [14,15] and nanoparticles (NPs) [16]. Generally, nanofillers with a high aspect ratio are favorable because they can form a conductive network in polymers at lower loadings and endow the nanocomposites with a strain sensing capability. However, it is noteworthy that increased aspect ratio will make it more difficult to homogeneously disperse these nanofillers in a matrix due to increased entanglements and Van der Waals force. Ecoflex [17], polydimethylsiloxane (PDMS) [18], rubber [19,20] and thermoplastic elastomers (TPEs) [21] are the most commonly utilized flexible substrates. To date, flexible strain sensors have achieved either high sensitivity or large workable strain range [22,23] but generally not simultaneously.

Recently however, various approaches have been reported to fabricate more flexible and sensitive strain sensors, including printing technology [24,25], micromolding [26] and chemical synthesis [27]. Flexible strain sensors prepared by coating processes have also been reported [28–30]. For example, Zhang et al. [29] made sensors based on a spandex yarn substrate with a MWCNTs coating, where the effects of nanotube concentration on the electrical resistance and electromechanical response reversibility were investigated. Wu et al. [30] prepared flexible, sensitive and washable strain sensors based on polyurethane (PU) yarn using a layer-by-layer (LBL) coating technique by alternately dipping PU yarn into negatively charged CB/cellulose nanocrystals/natural rubber suspension and positively charged chitosan solution. Park et al. [31] produced highly stretchable and wearable

* Corresponding authors.
*E-mail addresses:* dxiang01@hotmail.com (D. Xiang), yuntaoli@swpu.edu.cn (Y. Li).

https://doi.org/10.1016/j.compositesa.2018.06.009
Received 1 April 2018; Received in revised form 5 June 2018; Accepted 6 June 2018
Available online 07 June 2018
1359-835X/ 

graphene strain sensors via LBL coating of poly (vinyl alcohol) (PVA) and GNP onto three types of stretchable yarns (rubber (RY), nylon covered rubber (NCRY) and wool (WY)). Although these flexible strain sensors can exhibit high sensitivity, large workable range and promising application prospects, surprisingly little attention has been devoted to the scale up of processes to make such devices so that they will be economically viable. In addition, studies of ultraviolet aging, important for normal service conditions, assessment of actual applications for devices and sensing mechanisms are lacking.

In this work, we demonstrate a low-cost, simple and efficient approach for manufacturing stretchable and wearable strain sensors. TPU/MWCNT composites were coated onto the surface of spandex fiber using a LBL coating technique (Spandex is also a TPU so will be compatible with the coating). This resulted in an ultrathin layer of conductive composite material on the surface of the spandex fibers. This strategy only required low concentrations of MWCNTs and uniform coating layer thickness was achieved. Spandex was chosen as the coating substrate due to its large extensibility, excellent flexibility and good adhesion to carbon nanofillers. Additionally, commercially available spandex fibers can be readily incorporated into clothing or wearable equipment. In order to investigate the durability of this fiber sensor, an ultraviolet aging experiment was designed to explore the influence of ultraviolet irradiation time on the sensing performance. Additionally, a modeling study was conducted to understand the strain sensing mechanism. Finally, application of the sensor in monitoring diverse human motion, facial micro expressions and speech recognition are demonstrated.

## 2. Experimental section

### 2.1. Materials

Multi-walled carbon nanotubes (NC7000) were obtained from Nanocyl SA (Belgium). The MWCNTs have a nominal average length of 1.5 μm and a nominal diameter of 9.5 nm. The density of the MWCNTs is 1.85 g/cm$^3$. TPU powder (Elastollan 1185A) was supplied by BASF Co. Ltd. with a melt flow index of 17.5 g per 10 min (215 °C, at a pressure of 10 kg) and a density of 1.12 g/cm$^3$. Commercially available spandex fibers (Lycra, 840 dtex) were purchased from DuPont company. Dimethylformamid (DMF) reagent was purchased from Chengdu Kelong Chemical Reagent Company (China).

### 2.2. Preparation of the MWCNTs/TPU nanocomposite films and coating solution

In order to determine the required MWCNT concentration for a conductive coating, MWCNTs/TPU nanocomposite films with different MWCNT loading were fabricated and the electrical percolation threshold determined. Firstly, the MWCNTs were dispersed in DMF via ultrasonicating at 100 W and 40 kHz for 2 h at room temperature. TPU powder was dissolved in the resulting suspension by magnetic stirring for about 1 h. The mixed suspension was ultrasonicated for another 2 h and was transferred into a glass container (100 mm × 100 mm × 10 mm) to dry at 80 °C under vacuum for 24 h (Fig. 1a). The details of each solution formulation are shown in Table 1.

### 2.3. Fabrication of the fiber strain sensor

The prepared nanocomposite coating solution was poured into the coating bath of a custom-built fiber coater, in which the coating speed was controlled by a servo motor attached to a winding roll (Fig. 1b). The spandex fiber was guided into the coating bath by three small rollers. After coating, the fiber entered a heated stainless steel tube, which acted as a drying oven with the temperature control at 150 ± 5 °C. The speed of both rolling-up and unwinding was set at 2 rpm/min. The coating process was repeated as necessary to achieve the required number of layers (N). The core-wall structure of a coated fiber is illustrated in Fig. 1c. Finally, the coated fiber was cut into 80 mm segments for subsequent characterization.

### 2.4. Characterization

The surface morphology of the fiber sensor was studied using a JSM-7500F field-emission scanning electron microscopy (FE-SEM) at an accelerating voltage of 15 kV. Prior to FE-SEM, all samples were sputtered with gold (except the inset in Fig. 5c). The electrical conductivity (σ) of the MWCNTs/TPU nanocomposite films, dimensions equal to 80 mm × 10 mm × 0.2 mm), was measured using a two-point method combined with a picoamp-meter (Keithley 6485) and digital source meter (Tektronix PWS4323) at 3 V. The electrical conductivity of the nanocomposite films was calculated using Eq. (1):

$$\sigma = \frac{L}{RS} \tag{1}$$

where R is the electrical resistance of the sample, L and S are the length and cross-sectional area of the sample, respectively.

The conductivity of the coated fiber was also was measured via the two-point method on 30 mm long fibers. In the middle of this fiber segment, silver paste was applied to dissipate the contact resistance and to obtain a steady signal output. The conductive silver paste was connected with silver wires (see Fig. 2a). The cross-sectional area of the coated fibers was difficult to measure directly so the resistivity of the coated fiber was calculated. Due to the small thickness of the coating layer, the conductivity of the nanocomposite coating can be approximately calculated using Eq. (2):

$$\sigma = \frac{L}{RS} = \frac{\rho L^2}{Rm} \tag{2}$$

where L is length, R is the resistance of the sample, ρ is the density of the nanocomposite and m is the mass of the coating layer, calculated as Eq. (3):

$$m = m_{fiber} - m_0 \tag{3}$$

where $m_{fiber}$ and $m_0$ are the mass of the coated and original fibers, respectively.

The electromechanical performance of the fiber strain sensors was measured using a universal tester (MTS CMT4104) combined with a picoamp-meter and a digital source meter at a fixed voltage of 3 V (Fig. 2b). In order to investigate the durability of the fibres under typical environmental service conditions, the coated fibers were placed into a UV accelerated aging chamber with a power of 60 W applied for one and two weeks respectively. The wavelength of UV-light was 313 nm.

## 3. Results and discussion

### 3.1. Electrical conductivity of MWCNTs/TPU nanocomposite films and coated fibers

The percolation curve for the MWCNTs/TPU composite film is shown in Fig. 3. The electrical conductivity shows a drastic increase when the conductive nanofiller loading increases beyond a critical concentration. For example, the electrical conductivity increases from $10^{-8}$ to $10^{-3}$ S/m when the MWCNTs content increases from 0.1 wt% to 1 wt%. With further increases in the content of MWCNTs, the conductivity increased steadily up to $10^{-2}$ S/m and then levelled off indicating the formation of a robust MWCNT conductive network in the TPU matrix. The experimental data were fitted using classical percolation theory as expressed in Eq. (4) [32]:

$$\sigma = \sigma_0 (P - P_c)^t \tag{4}$$

where σ is the conductivity of the nanocomposite films, $\sigma_0$ is a constant

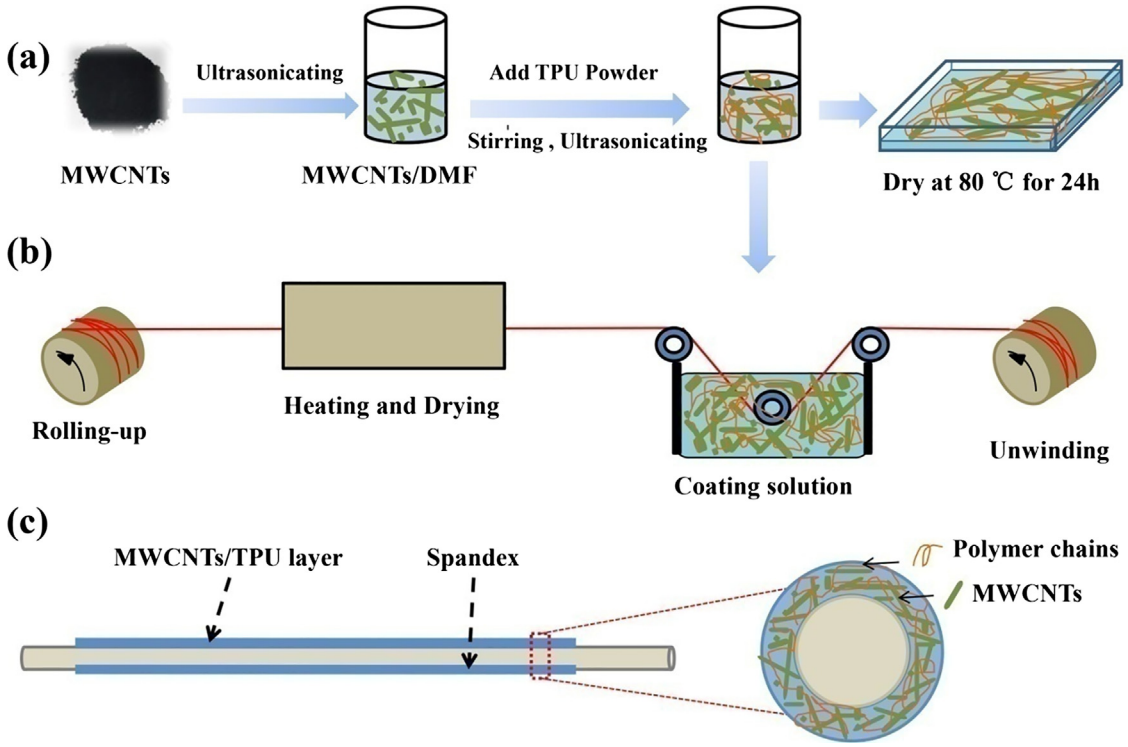


**Fig. 1.** Schematic of the strain sensing fiber fabrication using a LBL coating technique: (a) the preparation process for the coating solution and nanocomposite film, (b) the fiber coating process and setup, (c) schematic illustration of the fiber strain sensor.

**Table 1**
Solution components and quantities for preparation of MWCNTs/TPU nanocomposite films and LBL coatings.

| Sample No. | MWCNTs (g) | TPU (g) | DMF (g) | $C_{MWCNTs\text{-}CPC}$ (wt. %)[a] | $C_{CPC\text{-}sol}$ (wt. %)[b] |
|---|---|---|---|---|---|
| 1 | 0.002 | 1.998 | 25 | 0.1 | 8 |
| 2 | 0.006 | 1.994 | 25 | 0.3 | 8 |
| 3 | 0.010 | 1.990 | 25 | 0.5 | 8 |
| 4 | 0.020 | 1.980 | 25 | 1 | 8 |
| 5 | 0.040 | 1.960 | 25 | 2 | 8 |
| 6 | 0.060 | 1.940 | 25 | 3 | 8 |
| 7 | 0.080 | 1.920 | 25 | 4 | 8 |
| 8 | 0.100 | 1.900 | 25 | 5 | 8 |

[a] $C_{MWCNTs\text{-}CPC}$ is the MWCNTs concentration in the conductive nanocomposite film.

[b] $C_{CPC\text{-}sol}$ is the conductive nanocomposite concentration in the solution for LBL coating.

related to the scaling factor, P is the nanofiller content, $P_c$ is the critical content of the nanofiller and t is a critical exponent related to the dimensionality of conductive network. The percolation threshold of the nanocomposite was calculated to be only 0.1 wt%, which is much lower than most reported values [33,34]. In addition, the value of t for the MWCNT/TPU composites was estimated to be 2.79± 0.17 (see inset of Fig. 3) based on the fitting results. It is known that values of t equal to approximately 1.6–2 correspond to a three-dimensional conductive network system, and when values are 1–1.3 they are attributed to a two-dimensional system [35]. Many experimental studies [36–38] are in good agreement with these theoretical results, but the critical exponent t is not universal for some practical systems. The percolation bond model for chemically modified graphene/PS nanocomposites [39] resulted in t = 2.7±0.2. Higher values of critical exponent (> 3) have also been reported [40] for surface-modified carbon nanofiber/polyimide nanocomposites. A high value of t is attributed to the specific distributions of both conducting and insulating phases [41], and could

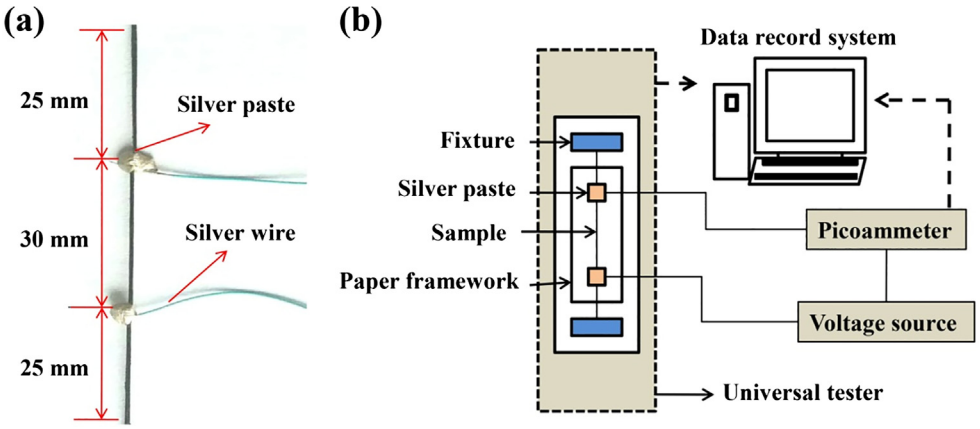


**Fig. 2.** (a) sample for strain sensing test and (b) schematic for strain sensing test.

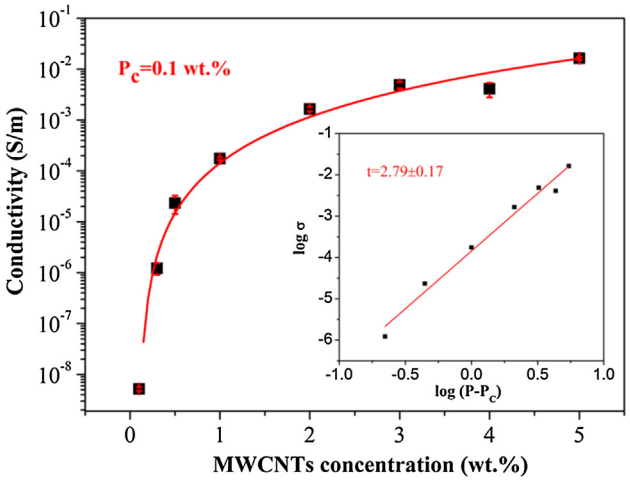


**Fig. 3.** Electrical conductivity of the MWCNT/TPU nanocomposite films. The inset shows the log − log plot of the conductivity as a function of $\log(P-P_c)$.

be an indication of electron transport behavior. Thus, the critical exponent value of the presented nanocomposite systems is deemed reasonable.

Based on the results above, the nanocomposite with 3 wt% MWCNTs was selected for the coating solution due to its stable conductivity. As shown in Fig. 4, the conductivity of the coated fibers increases with as the number of coating layers increases and plateaus after three layers due to the numerous conductive pathways formed on the surface of the spandex fibers. From these results it is possible to see that the conductivity of the sensor can be tuned depending on the number of layers applied.

### 3.2. Morphology of coated fibers

FE-SEM was used to observe the surface morphology of the neat and coated fibers. As shown in Fig. 5a, the original spandex consists of many microfibers with smooth surfaces and has an overall diameter of 610 ± 4 μm. The coating thickness of the fiber increases with the number of LBL cycles. As is clearly seen in Fig. 5(b–d), the boundaries of the individual microfibers become increasingly blurred as the coating is added and surface roughness increases, particularly for the 5 times coated sample (Fig. 5d). Numerous nanotubes can be clearly observed in the inset of Fig. 5c and a conductive network is formed in the polymer matrix. It should be noted that the sample shown in the inset of Fig. 5c is not gold-sputtered. The CNTs in the composite can therefore

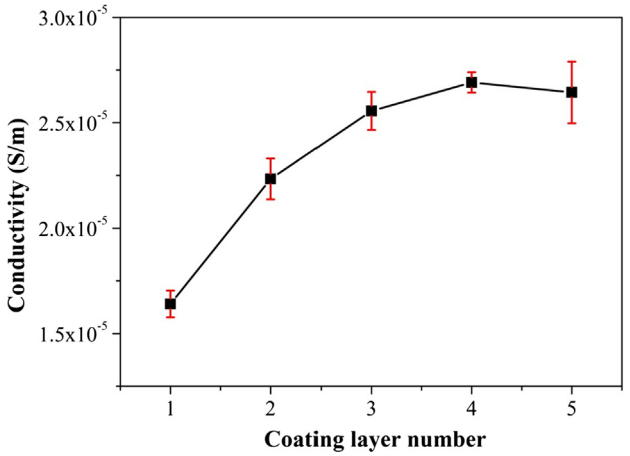


**Fig. 4.** Electrical resistivity of coated fibers as a function of the number of the coating layers.

be charged under the high accelerating voltage (15 kV) and emit enriched secondary electrons, which makes them visible [29].

### 3.3. Electromechanical performance of the nanocomposite coated fibers

The electromechanical performance characterization of the coated fibers was carried out by measuring the resistance under monodirectional and cyclic (stretching/releasing) loading. The gauge factor (GF) was calculated using Eq. (5) based on the relative resistance change ($\Delta R/R_0$) and tensile strain:

$$GF = \frac{\Delta R/R_0}{\Delta \varepsilon} \quad (5)$$

where $R_0$, $\Delta R$, and $\Delta\varepsilon$ represent the initial resistance without strain, resistance change with strain and applied strain, respectively. Fig. 6 shows relative resistance change of the fiber sensors with different coating number (N) as a function of tensile strain. The coated fiber sensors exhibit a steady increase in resistance under monodirectional loading, indicating an excellent electromechanical response. However, the value of $\Delta R/R_0$ decreases as the coating number increases from 132.2% (1 layer) to 19.8% (5 layers) at a strain of 5%, indicating that the sensitivity of the fiber strain sensor can be tuned by varying the number of conductive nanocomposite layers. The values of GF are obtained from the slopes of $\Delta R/R_0$-strain curves. It can be observed that the GF decreases from 26.4 (1 layer) to 8.1 (5 layers) at a strain of 5%. However, the 5 layer coated fiber also shows a high GF of 35217.1 at a higher strain range of 220–240% (see Fig. S1, supporting information). Furthermore, the nanocomposite coated fiber sensors exhibit a larger workable strain range as the number of coating layers increases, e.g., it increases from 80% to ~240% when the coating number increases from 1 to 5. The fiber sensors with a greater number of layers exhibit a lower sensitivity and larger workable strain range because a robust conductive network forms when more MWCNTs overlap and entangle with each other with an increasing number of layers. Hence, the 5 layer coated fiber sensor exhibits a smaller resistance change compared with the 1 layer coated fiber sensor under the same strain. Further analysis of the sensing mechanism is presented in Section 3.4. In general, the coated fiber sensors show an excellent performance in terms of sensitivity and workable strain range compared with recently reported strain sensors (see Fig. 7) [1–3,14,17,42–50]. In addition, the conductive nanocomposite is just coated on the surface of fibers without damaging the original fiber structure, thus the high stretchability is retained despite some possible nanotube agglomerates in the thin nanocomposite coating.

To further investigate the influence of coating number on the performance of the fiber sensors, sensors with different numbers of layers (N = 1, 3, 5) were tested under a cyclic load with a strain of 30% and frequency of 0.2 Hz. Fig. 8 shows that the $\Delta R/R_0$ clearly decreases as the coating number increases. Additionally, a more obvious shoulder in the $\Delta R/R_0$ curve is observed for the fiber sensor coated with one layer (N = 1) compared with the (N = 3, 5) sensors. The formation of the shoulder can be explained by a competition between the destruction and reconstruction of the conductive network in the nanocomposite coating during stretching and release. The sensitivity of fiber sensor with 5 layers is the lowest which is in keeping with the monodirectional tensile results.

Fig. 9 shows the relative resistance change of the strain sensors at a cyclic strain of 30% and frequencies of 0.01, 0.1, 0.2 and 1 Hz. All the sensors exhibit excellent responses within this wide testing frequency range. $\Delta R/R_0$ increases as the frequency increases indicating frequency dependence. The stiffer mechanical response upon increasing the strain frequency is attributed to the reduction of molecular mobility of polymer chains [51].

To examine the stability and repeatability of the strain sensing behavior, more cyclic stretching/releasing tests (up to 2000 cycles) were performed at a strain of 30% and a frequency of 1 Hz. It can be seen in

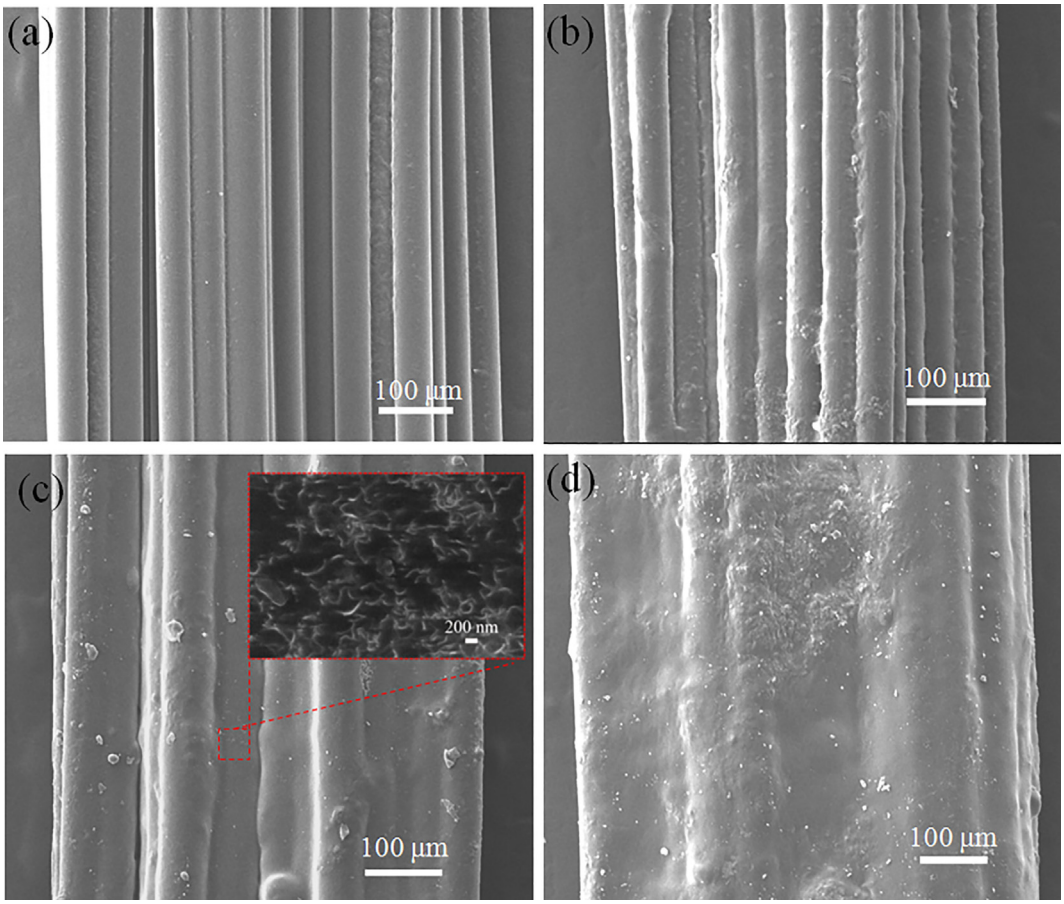


**Fig. 5.** SEM images of (a) the original spandex fiber and (b-d) nanocomposite coated fibers with different number of LBL coating layers: (b) 1 layer, (c) 3 layers, (d) 5 layers.

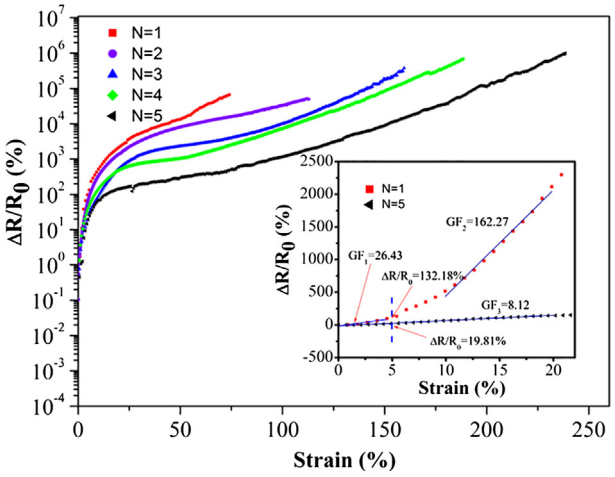


**Fig. 6.** Relative resistance change of the fiber sensors with different coating number as a function of tensile strain.

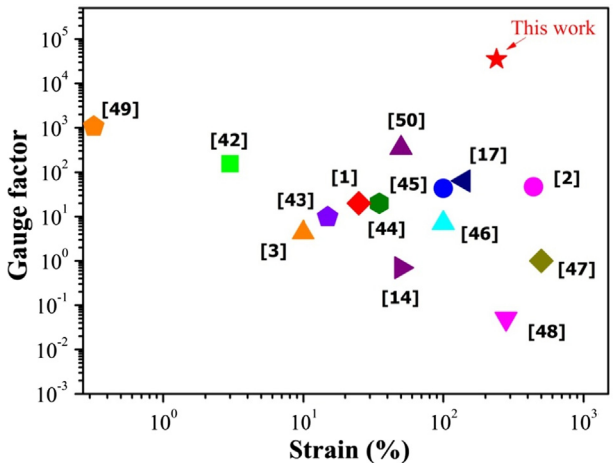


**Fig. 7.** Comparison of the gauge factor and workable strain range of the coated spandex strain sensor with that of recently reported flexible strain sensors.

Fig. 10 that the $\Delta R/R_0$ of all the samples decreases to different extents during the first 200 cycles, stabilizing afterwards. This can be attributed to the conductive network in the nanocomposite coating of fiber surface reaching a more stable state. One can see that all the tested fibers exhibit an excellent stability in strain sensing even after 2000 testing cycles.

Based on the sensing performance above, the fiber sensor with 3 layers was selected to test its performance under cyclic loading at different strains and a frequency of 0.2 Hz. As shown in Fig. 11a, the $\Delta R/R_0$ of the sensor responds consistently to the loading cycles at strains of 5%, 10%, 30%, 50% and 80%, indicating that the coated fiber is capable of sensing multiple strain deformations. In addition, it can be observed that the shoulder peak is enhanced when the strain increases. Double peaks of $\Delta R/R_0$ during a single loading have rarely been reported in conductive polymer composites [52]. The behavior is often explained by competing mechanisms such as destruction and reconstruction of conductive network during stretching/releasing [53]. Mechanical hysteresis is proposed to explain the phenomenon whereby the retraction of the polymer chains causes some of the conductive

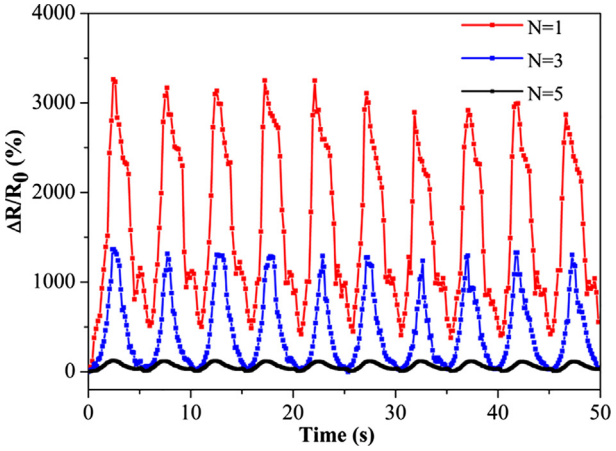


**Fig. 8.** Relative resistance change of the strain sensors with different coating numbers (N = 1, 3 and 5) at a cyclic strain of 30% and a frequency of 0.2 Hz.

networks to re-form after the large strain deformation [54]. Not all of the polymer chains return to their initial state after the load is removed. This hysteresis leads to a greater destruction of the MWCNT conductive pathways, resulting in the shoulder peak increasing, as deformation increases.

Since most wearable smart devices or textiles will eventually be exposed to sunlight, which potentially can accelerate aging and eventual failure of the sensor material, we conducted ultraviolet aging experiments to investigate the influence of UV irradiation on the sensing performance. Fig. 11b and c show the $\Delta R/R_0$ of sensors exposed to UV for one and two weeks under cyclic loading at different strains. One can see in Fig. 11b that UV irradiation for one week slightly affects the sensing performance, with the shoulder becoming much more obvious at a cyclic strain of 80%. After UV irradiation for two weeks, the shape of the peaks becomes less regular at strains exceeding 30% (Fig. 11c). A possible reason for this behavior is that the longer exposure to ultraviolet irradiation accelerates the aging of the fiber surface, and the subsequent evolution of surface microcracks (Fig. 12d) during stretching/releasing leads to sudden changes in the conductive network. The $\Delta R/R_0$ also increases when the strain exceeds 30%, indicating a higher sensitivity, particularly for the sensor exposed to UV-light for two weeks. In general, stable electromechanical responses are still retained for the coated fibers despite being exposed to long-term and strong UV irradiation. This indicates that the fiber sensors have a stable sensing performance.

The surface morphology of the UV exposed fiber sensors before and after a cyclic strain of 30% was characterized using FE-SEM (see Fig. 12). There is no significant difference for the 3 layer fiber sensor after UV treatment compared to the unexposed sensor (Fig. 5c). However, many surface microcracks can be clearly observed on sensors exposed for 2 weeks after 100 stretching/releasing cycles (see Fig. 12d). The width of these microcracks reaches 3 μm. Hence, the increased $\Delta R/R_0$ and sensitivity of the UV treated sensors can be attributed to microcrack propagation [55] facilitating the destruction of conductive network as postulated above. The coating layers of the fiber sensor become more brittle after prolonged exposure to strong UV irradiation and microcracks form at the stress concentration sites to release the stress upon stretching. Stretching leads to enlargement of the microcracks on the surface layer and the separation of the microcrack edges inhibits electrical conduction. The 3 layer sensor does not show obvious surface microcracks even after 2000 cycles (see Fig. 12c) which demonstrates that the duration of the UV treatment is a significant factor in the appearance of the microcracks. Although long-term UV irradiation could result in a mechanical deterioration of the coating on the fiber surface (see Fig. S2, supporting information), the nanocomposite coating still strongly adheres to the spandex fiber even after large deformation indicating good durability of the nanocomposite coated fiber sensors.

### 3.4. Modeling and mechanism

As discussed above, deformation of the conductive network plays a key role in the electromechanical response of the coated fiber. In order to better understand the sensing mechanism, a modeling study was carried out. According to the model [56] derived from tunneling theory by Simmons [57], the total resistance R of a coated fiber can be calculated using Eq. (6):

$$R = \left(\frac{L}{N}\right)\left(\frac{8\pi hs}{3\gamma a^2 e^2}\right)\exp(\gamma s) \tag{6}$$

$$\gamma = \frac{4\pi\sqrt{2m\varphi}}{h} \tag{7}$$

where L is the number of particles forming a single conductive path, N is the number of conductive paths, h is Planck's constant, s is the

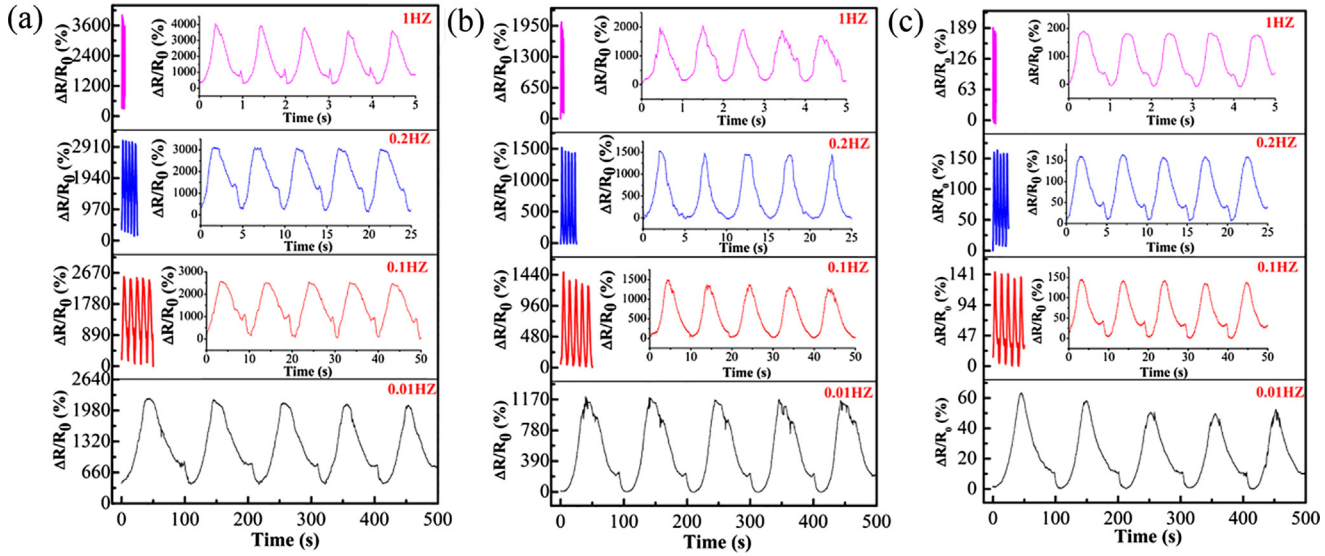


**Fig. 9.** Relative resistance of the strain sensors with different layers (N) at a cyclic strain of 30% and a frequency of 0.01, 0.1, 0.2 and 1 Hz: (a) N = 1, (b) N = 3, (c) N = 5.

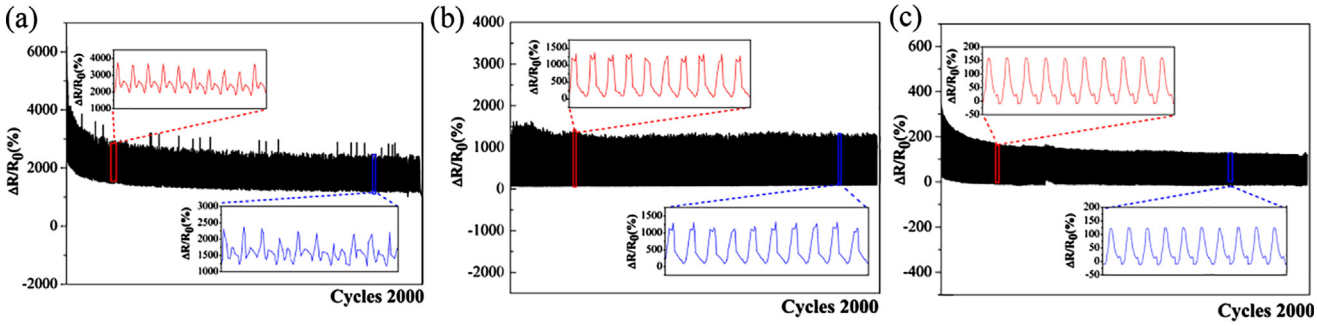


**Fig. 10.** Relative resistance of the strain sensors with different layer numbers (N) during 2000 cycles at a strain of 30% and a frequency of 1 Hz: (a) N = 1, (b) N = 3, (c) N = 5.

shortest distance between conductive particles, $a^2$ is the effective cross-section area, e is the electron charge, m is the electron mass, and φ is the height of the potential barrier between particles.

Due to the separation of the conductive particles and changes of the inter-particle distance under strain, the resistance of the coated fiber will be altered. The inter-particle distance will vary linearly and proportionally with strain increases from $s_0$ to s hence, it can be expressed as in Eq. (8):

$$S = S_0\left(1 + C\left(\frac{\Delta l}{l_0}\right)\right) = S_0(1 + C\varepsilon) \tag{8}$$

where $l_0$in the initial length, Δlis the deformation length, εis tensile strain of the coated fiber, and C is a constant with a different value in different material systems.

The non-linear rate of resistivity increase at larger strains indicates a non-linear response for the number of conductive pathways (N) at large strains. This can be represented by Eq. (9):

$$N = \frac{N_0}{\exp(M\varepsilon + W\varepsilon^2 + U\varepsilon^3 + V\varepsilon^4)} \tag{9}$$

where M, W, U, V are constants.

Substitution of Eqs. (8) and (9) into Eq. (6) gives Eq. (10):

$$R = B(1 + C\varepsilon)\exp[A + (M + AC)\varepsilon + W\varepsilon^2 + U\varepsilon^3 + V\varepsilon^4] \tag{10}$$

where$A = \gamma S_0$, $B = \frac{8\pi hns_0}{3\gamma N_0^2 e^2 a^2}$ , and n is the total number of conductive particles (n = L × N).

Fig. 13 demonstrates that this equation models the experimental data well. The fitting parameters A, B, C, M, W, U and V are listed in Table S1 (supporting information). Fig. 14a and b, show changes of the tunneling distance (change of TD, y = Cx) and the number of conductive pathways (change of CP, $y = Mx + Wx^2 + Ux^3 + Vx^4$) against strain [58]. The tunneling distance generally increases linearly with strain. It is observed that the changes of TD and CP in the 3 layer fiber increase at a higher rate compared with the 5 layer fiber. This models the experimental results whereby a lower sensitivity of the fiber sensor with a greater number of coating layers is observed. Furthermore, the changes of TD and CP for the UV treated samples also increase faster than for the untreated samples, indicating that the conductive networks in the UV treated samples deform significantly and are more readily destroyed under strain.

### 3.5. Applications

Spandex fibers are ideal for smart fabrics due to their high elasticity, commercial availability, design versatility and low cost. Therefore, the MWCNTs/TPU nanocomposite coated fibers developed here can be used as wearable sensors, and can be easily embedded into a garment without sacrificing flexibility. The large workable strain range should

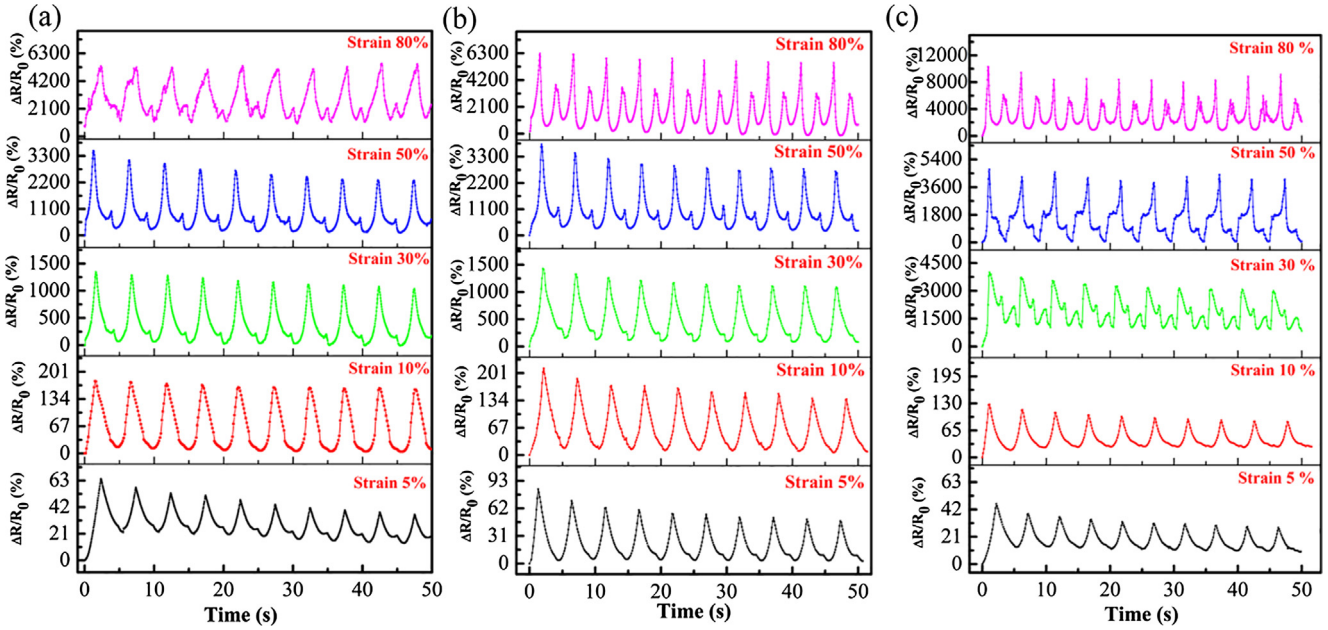


**Fig. 11.** Relative resistance of the coated fiber sensors (N = 3) under cyclic loading at different strains (5%, 10%, 30%, 50% and 80%) and a frequency of 0.2 Hz: (a) sensor without UV irradiation treatment; sensor exposed to UV-light for (b) one and (c) two weeks.

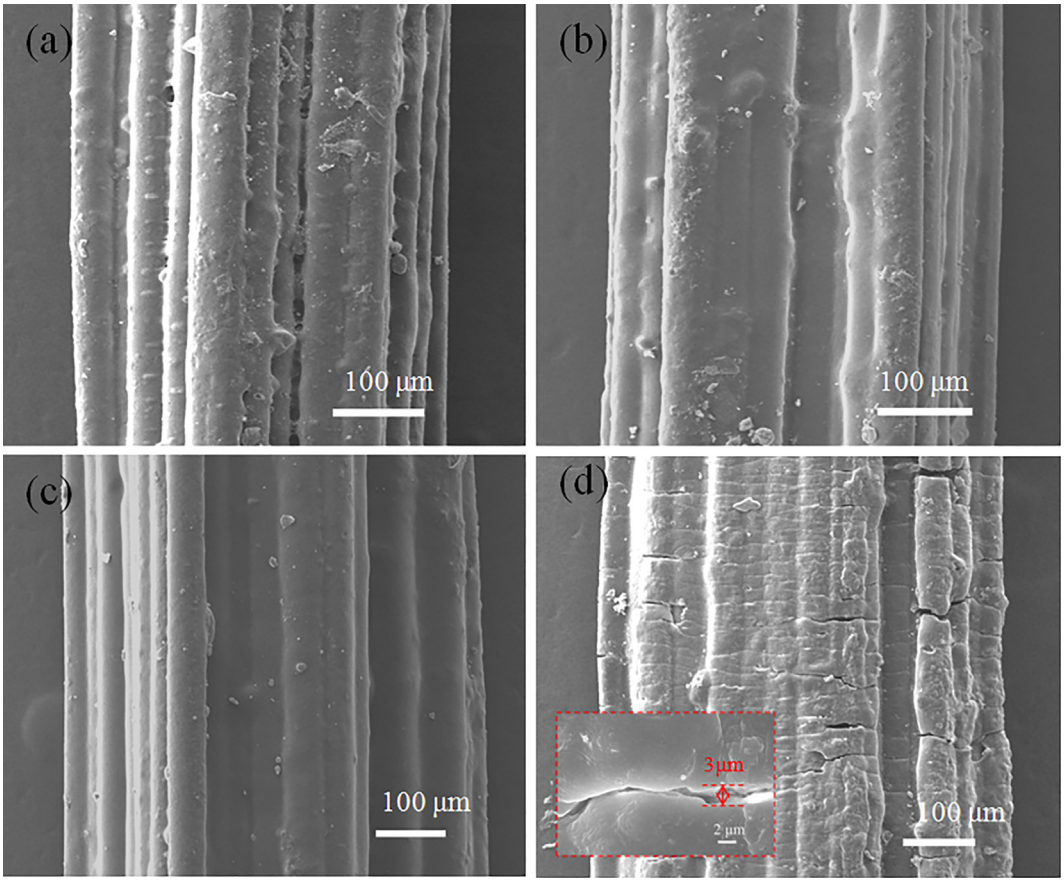


**Fig. 12.** SEM images of the UV treated fiber sensors (N = 3) before and after a 30% cyclic strain: exposed to UV-light for (a) one and (b) two weeks; (c) after 2000 cycles for the sensor without UV treatment, (d) after 100 cycles for the sensor exposed to UV-light for two weeks.

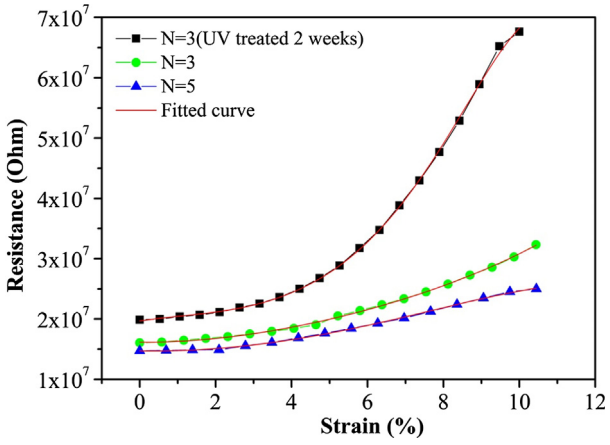


**Fig. 13.** Experimental (dots) and theoretical (red solid lines) results for strain-resistance relationship of the fiber sensors. (For interpretation of the references to colour in this figure legend, the reader is referred to the web version of this article.)

enable the fiber sensor to detect human body motion, such as the movements of the joints of fingers, wrists and knees.

As shown in Fig. 15a, when fixed on a finger joint, the fiber sensor could monitor motions at different bending angles. When the finger was bent to 30° and 90°, the $\Delta R/R_0$ of the sensor showed different peak intensities. Furthermore, when the extended finger continued to be bent for about 10 s, the $\Delta R/R_0$ of fiber sensor reached a certain value and remained stable (Fig. 15b). Further bending of the finger led to a stronger signal. Similar measurements were conducted on the wrist and knee joints with continual bending/extending, and the coated fiber demonstrated excellent sensing performance (see Fig. 15c and d). This demonstrates that the nanocomposite coated fiber has ability to monitor large movements.

Statistical research shows that people communicate ~7% of information verbally and 55% information is conveyed through facial expressions [59]. Therefore, the fiber sensor was fixed on the forehead, upper eyelid and face with the aid of bandage to investigate its capability for facial expression monitoring. As shown in Fig. 16a–c, when the person frowned, blinked and smiled, the sensor responded rapidly. When the facial expression returned to a relaxed state, the $\Delta R/R_0$ returned to its initial level. Repeated frowning, blinking and smiling produced continual signals confirming the good repeatability and stability of the nanocomposite coated fiber strain sensor. This fiber strain sensor was also used to examine its application in speech recognition (some results are shown in Fig. 16d). The sensor was first attached on the person's throat. When the person read different English words, the strain sensor showed a distinct signal pattern for each word attributed to the specific muscle movement and subtle pressure changes needed specifically for each word. This demonstrates a good sensing performance of the nanocomposite coated fiber strain sensor in monitoring delicate movements of human muscles.

## 4. Conclusions

In this study, we fabricated a highly flexible, stretchable and low-cost strain sensor using a layer-by-layer coating process to apply conductive MWCNT/TPU nanocomposite to commercial spandex fibers. The conductive pathways on the fiber surface can be readily tuned by the number of layer applied. The sensor exhibited high sensitivity

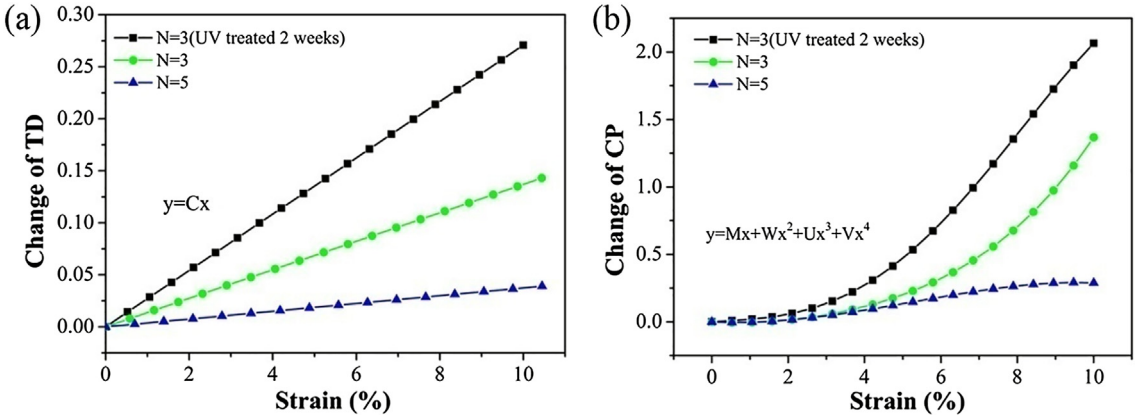


**Fig. 14.** Change of the (a) tunneling distance and (b) the conductive pathway as a function of strain for the fiber sensors.

(GF = 26.43 within strain of 0–5% for the sensor with one coating layer) and a wide workable strain range (0–240% for the sensor with five coating layers). Also, this sensor exhibited regular frequency responses within the test frequency range (0.01–1 Hz) indicating sensor potential for monitoring frequency changes. In cyclic stretching/releasing tests, shoulder peaks were observed in the $\Delta R/R_0$ results which were enhanced with an increase in the applied strain. The effect of UV irradiation on the sensing performance of the sensor was also investigated. It was observed that the sensitivity of the sensor increased with increasing irradiation duration due to the presence of microcracks on the fiber surface under stretching/releasing cycles, while stable electromechanical responses were retained. The nanocomposite coating firmly adhered to the surface of the fiber substrate despite the exposure to a strong UV-light for a long time. More research on the ultraviolet resistance of this sensor is anticipated in our future work with the goal to improve sensor service life. In addition, a modeling study based on tunneling theory was carried out to analyze the sensing mechanism of the coated fibres and the results agree well with experimental observations. Overall, this sensor exhibited excellent stability, repeatability and durability under repeatedly large deformations. We also demonstrated its ability to monitor and register human motions including the joint movements of the human body, facial micro expressions and speech recognition.

## Acknowledgements

This work is supported by Sichuan Science and Technology Program (2017HH0086, 2017JY0152), Education Department of Sichuan

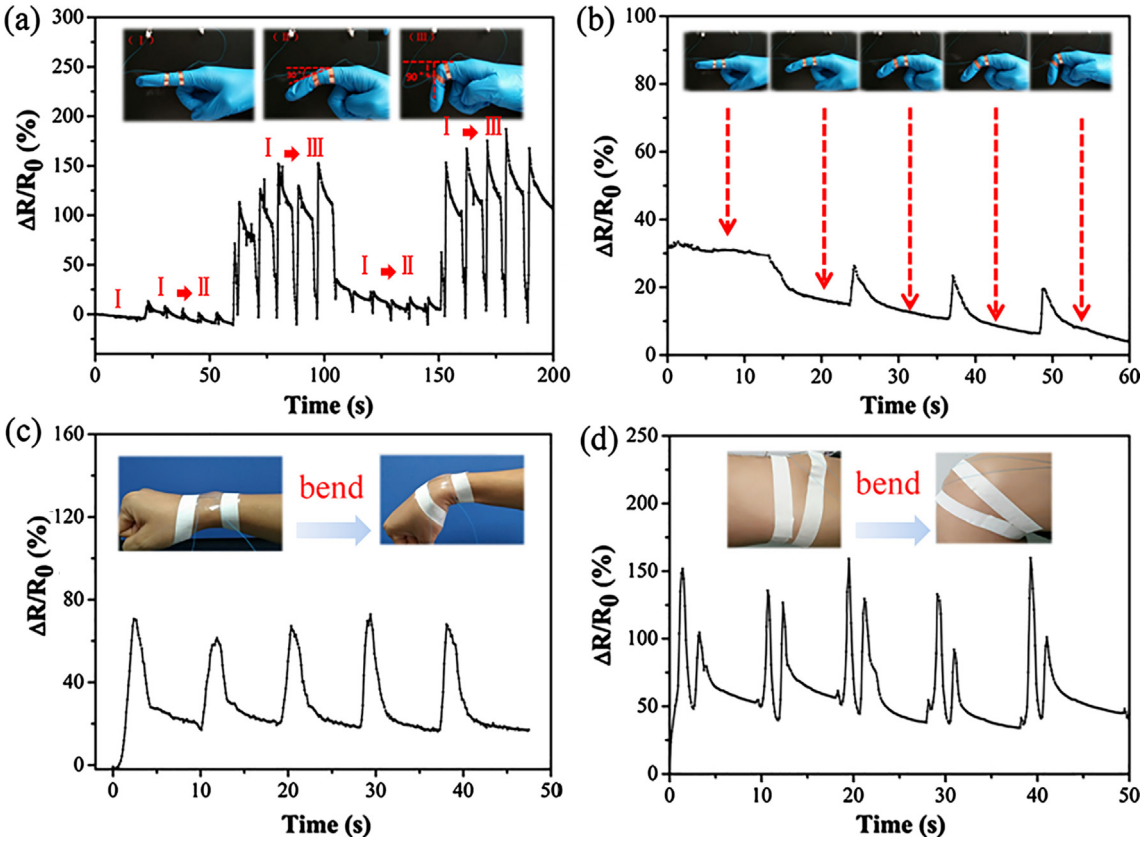


**Fig. 15.** Recording of human motions using the nanocomposite coated fiber sensor with three layers (N = 3): (a) bending and unbending of the index finger at 30° and 90°, (b) the index finger remained bent at different angles for about 10 s; detection of the (c) wrist and (d) knee motions.

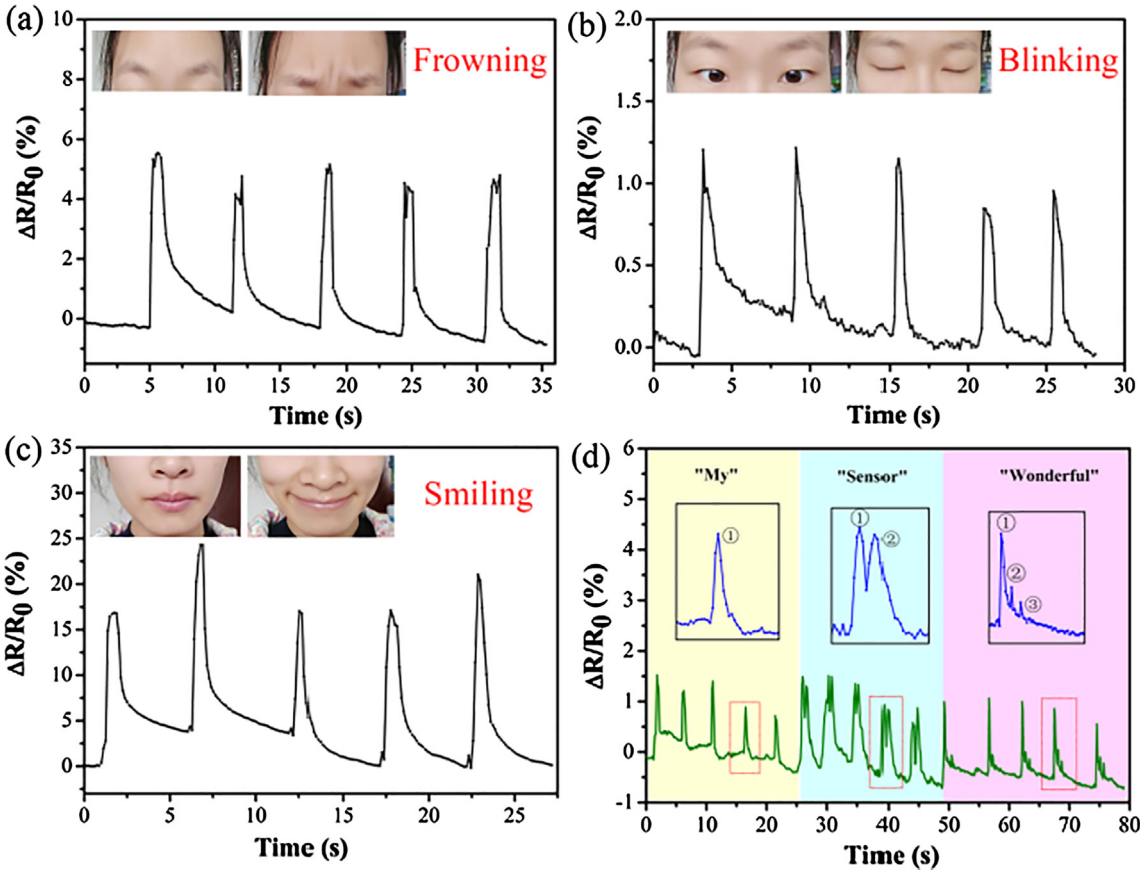


**Fig. 16.** Electromechanical responses of the fiber sensor to repeated (a) frowning, (b) blinking, (c) smiling and (d) speaking; in (d) the person pronounced words "my", "sensor", and "wonderful".

Province (17ZB0462) and Open Experimental Program of SWPU (KSZ17121).

## Appendix A. Supplementary material

Supplementary data associated with this article can be found, in the online version, at https://doi.org/10.1016/j.compositesa.2018.06.009.

## References

[1] Zheng Q, Liu X, Xu H, Cheung MS, Choi YW, Huang HC, et al. Sliced graphene foam films for dual-functional wearable strain sensors and switches. Nanoscale Horizons 2017;3.
[2] Ryu S, Lee P, Chou JB, Xu R, Zhao R, Hart AJ, et al. Fabrication of extremely elastic wearable strain sensor using aligned carbon nanotube fibers for monitoring human motion. ACS Nano 2015;9:5929–36.
[3] Zheng Y, Li Y, Li Z, Wang Y, Dai K, Zheng G, et al. The effect of filler dimensionality on the electromechanical performance of polydimethylsiloxane based conductive nanocomposites for flexible strain sensors. Compos Sci Technol 2017;139:64–73.
[4] Pan Y, Liu X, Hao X, Schubert DW. Conductivity and phase morphology of carbon black-filled immiscible polymer blends under creep: an experimental and theoretical study. PCCP 2016;18:32125–31.
[5] Ma PC, Kim JK, Tang BZ. Effects of silane functionalization on the properties of carbon nanotube/epoxy nanocomposites. Compos Sci Technol 2007;67:2965–72.
[6] Gao L, Thostenson ET, Zhang Z, Chou TW. Sensing of damage mechanisms in fiber-reinforced composites under cyclic loading using carbon nanotubes. Adv Funct Mater 2010;19:123–30.
[7] Chen J, Cui X, Zhu Y, Jiang W, Sui K. Design of superior conductive polymer composite with precisely controlling carbon nanotubes at the interface of a co-continuous polymer blend via a balance of π-π interactions and dipole-dipole interactions. Carbon 2017;114:441–8.
[8] Xiang D, Wang L, Tang Y, Zhao C, Harkin-Jones E, Li Y. Effect of phase transitions on the electrical properties of polymer/carbon nanotube and polymer/graphene nanoplatelet composites with different conductive network structures. Polym Int 2018;67:227–35.
[9] Hempel M, Nezich D, Kong J, Hofmann M. A novel class of strain gauges based on layered percolative films of 2D materials. Nano Lett 2012;12:5714–8.
[10] Huang J, Zhu Y, Xu L, Chen J, Jiang W, Nie X. Massive enhancement in the thermal conductivity of polymer composites by trapping graphene at the interface of a polymer blend. Compos Sci Technol 2016;129:160–5.
[11] Cheng Y, Wang R, Sun J, Gao L. A Stretchable and Highly Sensitive Graphene-Based Fiber for Sensing Tensile Strain, Bending, and Torsion. Adv Mater 2016;27:7365–71.
[12] Jang H, Park YJ, Chen X, Das T, Kim MS, Ahn JH. Graphene-based flexible and stretchable electronics. Adv Mater 2016;28:4184–202.
[13] Chen L, Chen GH, Lu L. Piezoresistive Behavior Study on Finger-Sensing Silicone Rubber/Graphite Nanosheet Nanocomposites. Adv Funct Mater 2010;17:898–904.
[14] Yao S, Zhu Y. Wearable multifunctional sensors using printed stretchable conductors made of silver nanowires. Nanoscale 2014;6:2345–52.
[15] Amjadi M, Pichitpajongkit A, Lee S, Ryu S, Park I. Highly stretchable and sensitive strain sensor based on silver nanowire-elastomer nanocomposite. ACS Nano 2014;8:5154–63.
[16] Lee JH, Yang D, Kim S, Park I. Stretchable strain sensor based on metal nanoparticle thin film for human motion detection & flexible pressure sensing devices. Nanoscale 2014;6:11932–9.
[17] Zhang M, Wang C, Wang H, Jian M, Hao X, Zhang Y. Carbonized Cotton Fabric for High-Performance Wearable Strain Sensors. Adv Funct Mater 2017;27.
[18] Bae S-H, Lee Y, Sharma BK, Lee H-J, Kim J-H, Ahn J-H. Graphene-based transparent strain sensor. Carbon 2013;51:236–42.
[19] Li Z, Li L, Mo L, Wang Z, Yang W, Zhou H, et al. Highly Sensitive Flexible Pressure Sensor with Microstructural Dielectric Layer. In: China academic conference on printing & packaging and media technology; 2016, p. 1087–94.
[20] Boland CS, Khan U, Backes C, O'Neill A, Mccauley J, Duane S, et al. Sensitive, high-strain, high-rate bodily motion sensors based on graphene-rubber composites. Acs Nano 2014;8:8819–30.
[21] Tadakaluru S, Thongsuwan W, Singjai P. Stretchable and flexible high-strain sensors made using carbon nanotubes and graphite films on natural rubber. Sensors 2014;14:86–876.
[22] Trung TQ, Ramasundaram S, Hwang BU, Lee NE. An All-Elastomeric Transparent and Stretchable Temperature Sensor for Body-Attachable Wearable Electronics. Adv Mater 2016;28:502–9.
[23] Wang Y, Wang L, Yang T, Li X, Zang X, Zhu M, et al. Wearable and highly sensitive graphene strain sensors for human motion monitoring. Adv Funct Mater 2014;24:4666–70.
[24] Lee H, Seong B, Moon H, Byun D. Directly printed stretchable strain sensor based on ring and diamond shaped Silver nanowire electrodes. RSC Adv 2015;5:28379–84.
[25] Muth JT, Vogt DM, Truby RL, Mengüç Y, Kolesky DB, Wood RJ, et al. Embedded 3D

printing of strain sensors within highly stretchable elastomers. Adv Mater 2014;26:6307–12.
[26] Liu CX, Choi JW. Analyzing resistance response of embedded PDMS and carbon nanotubes composite under tensile strain. Microelectron Eng 2014;117:1–7.
[27] Cai L, Song L, Luan P, Zhang Q, Zhang N, Gao Q, et al. Super-stretchable, transparent carbon nanotube-based capacitive strain sensors for human motion detection. Sci Rep 2013;3:3048–56.
[28] Hu W, Niu X, Zhao R, Pei Q. Elastomeric transparent capacitive sensors based on an interpenetrating composite of silver nanowires and polyurethane. Appl Phys Lett 2013;102:1438–87.
[29] Zhang R, Deng H, Valenca R, Jin J, Fu Q, Bilotti E, et al. Carbon nanotube polymer coatings for textile yarns with good strain sensing capability. Sens Actuators, A 2012;179:83–91.
[30] Wu X, Han Y, Zhang X, Lu C. Highly sensitive, stretchable, and wash-durable strain sensor based on ultrathin conductive layer@polyurethane yarn for tiny motion monitoring. ACS Appl Mater Interfaces 2016;8:9936–45.
[31] Park JJ, Hyun WJ, Mun SC, Park YT, Park OO. Highly stretchable and wearable graphene strain sensors with controllable sensitivity for human motion monitoring. ACS Appl Mater Interfaces 2015;7:6317–24.
[32] Huang JC. Carbon black filled conducting polymers and polymer blends. Adv Polym Tech 2002;21:299–313.
[33] Zhao J, Dai K, Liu C, Zheng G, Wang B, Liu C, et al. A comparison between strain sensing behaviors of carbon black/polypropylene and carbon nanotubes/polypropylene electrically conductive composites. Compos A Appl Sci Manuf 2013;48:129–36.
[34] Huang J, Mao C, Zhu Y, Jiang W, Yang X. Control of carbon nanotubes at the interface of a co-continuous immiscible polymer blend to fabricate conductive composites with ultralow percolation thresholds. Carbon 2014;73:267–74.
[35] Gao JF, Li ZM, Meng QJ, Yang Q. CNTs/UHMWPE composites with a two-dimensional conductive network. Mater Lett 2008;62:3530–2.
[36] Xu J, Florkowski W, Gerhardt R, Moon Kyoungsik, Wong CP. Shear modulated percolation in carbon nanotube composites. J Phys Chem B 2006;110:12289–111292.
[37] Du J, Zhao L, Zeng Y, Zhang L, Li F, Liu P, et al. Comparison of electrical properties between multi-walled carbon nanotube and graphene nanosheet/high density polyethylene composites with a segregated network structure. Carbon 2011;49:1094–100.
[38] Xiang D, Harkin-Jones E, Linton D. Characterization and structure-property relationship of melt-mixed high density polyethylene/multi-walled carbon nanotube composites under extensional deformation. RSC Adv 2015;5:47555–68.
[39] Stankovich S, Dikin DA, Dommett GH, Kohlhaas KM, Zimney EJ, Stach EA, et al. Graphene-based composite materials. Nature 1990;442:282–6.
[40] Arlen MJ, Wang D, Jacobs JD, Justice R, Trionfi A, Hsu JWP, et al. Thermal – electrical character of in situ synthesized polyimide-grafted carbon nanofiber composites. Macromolecules 2015;41:8053–62.
[41] Kogut PM, Straley JP. Distribution-induced non-universality of the percolation conductivity exponents. J Phys C: Solid State Phys 1979;12:2151–60.
[42] Hu N, Itoi T, Akagi T, Kojima T, Xue J, Yan C, et al. Ultrasensitive strain sensors made from metal-coated carbon nanofiller/epoxy composites. Carbon 2013;51:202–12.
[43] Liu Z, Qi D, Guo P, Liu Y, Zhu B, Yang H, et al. Thickness-Gradient Films for High Gauge Factor Stretchable Strain Sensors. Adv Mater 2015;27:6230–7.
[44] Kim KK, Hong S, Cho HM, Lee J, Suh YD, Ham J, et al. Highly sensitive and stretchable multidimensional strain sensor with prestrained anisotropic metal nanowire percolation networks. Nano Lett 2015;15:5240–7.
[45] Wang S, Zhang X, Wu X, Lu C. Tailoring percolating conductive networks of natural rubber composites for flexible strain sensors via a cellulose nanocrystal templated assembly. Soft Matter 2015;12:845–52.
[46] Yan C, Wang J, Kang W, Cui M, Wang X, Foo CY, et al. Highly stretchable piezoresistive graphene-nanocellulose nanopaper for strain sensors. Adv Mater Weinheim 2014;26:2022–7.
[47] Amjadi M, Yoon YJ, Park I. Ultra-stretchable and skin-mountable strain sensors using carbon nanotubes-Ecoflex nanocomposites. Nanotechnology 2015;26:375501–12.
[48] Yamada T, Hayamizu Y, Yamamoto Y, Yomogida Y, Izadi-Najafabadi A, Futaba DN, et al. A stretchable carbon nanotube strain sensor for human-motion detection. Nat Nanotechnol 2011;6:296–301.
[49] Zhang BC, Wang H, Zhao Y, Li F, Ou XM, Sun BQ, et al. Large-scale assembly of highly sensitive Si-based flexible strain sensors for human motion monitoring. Nanoscale 2016;8:2123–8.
[50] Murugaraj P, Mainwaring D, Khelil NA, Peng JL, Siegele R, Sawant P. The improved electromechanical sensitivity of polymer thin films containing carbon clusters produced in situ by irradiation with metal ions. Carbon 2010;48:4230–7.
[51] Li YQ, Zhu WB, Yu XG, Huang P, Fu SY, Hu N, et al. Multifunctional wearable device based on flexible and conductive carbon sponge/polydimethylsiloxane composite. ACS Appl Mater Interfaces 2016;8:33189–96.
[52] Cravanzola S, Haznedar G, Scarano D. Carbon-based piezoresistive polymer composites: structure and electrical properties. Carbon 2013;62:270–7.
[53] Zhang R, Deng H, Valenca R, Jin J, Fu Q, Bilotti E, et al. Strain sensing behaviour of elastomeric composite films containing carbon nanotubes under cyclic loading. Compos Sci Technol 2013;74:1–5.
[54] Lozano-Pérez C, Cauich-Rodríguez JV, Avilés F. Influence of rigid segment and carbon nanotube concentration on the cyclic piezoresistive and hysteretic behavior of multiwall carbon nanotube/segmented polyurethane composites. Compos Sci Technol 2016;128:25–32.
[55] Li M, Li H, Zhong W, Zhao Q, Wang D. Stretchable conductive polypyrrole/polyurethane (PPy/PU) strain sensor with netlike microcracks for human breath detection. ACS Appl Mater Interfaces 2014;6:1313–9.
[56] Zhang XW, Pan Y, Zheng Q, Yi XS. Time dependence of piezoresistance for the conductor-filled polymer composites. J Polym Sci, Part B: Polym Phys 2000;38:2739–49.
[57] Simmons JG. Generalized formula for the electric tunnel effect between similar electrodes separated by a thin insulating film. J Appl Phys 1963;34:1793–803.
[58] Duan L, Fu S, Deng H, Zhang Q, Wang K, Chen F, et al. The resistivity-strain behavior of conductive polymer composites: stability and sensitivity. J Mater Chem A 2014;2:17085–98.
[59] Hu C, Chang Y, Feris R, Turk M. Manifold Based Analysis of Facial Expression. In: Computer vision and pattern recognition workshop, 2004. CVPRW '04. conference on.; 2005. p. 605–14.